



Molecular Characterization of the Coproduced Extracellular Vesicles in HEK293 during Virus-Like Particle Production

Jesús Lavado-García,* Irene González-Domínguez, Laura Cervera, Inmaculada Jorge, Jesús Vázquez, and Francesc Gòdia



Cite This: *J. Proteome Res.* 2020, 19, 4516–4532



Read Online

ACCESS |



Metrics & More



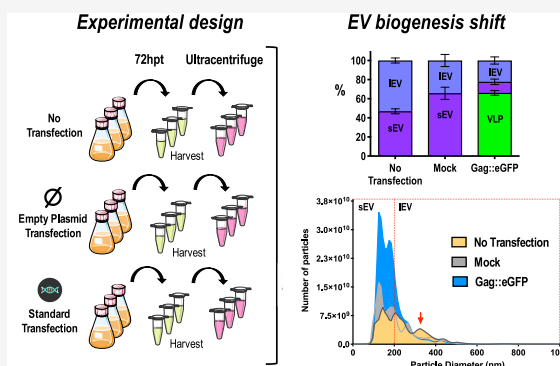
Article Recommendations



Supporting Information

ABSTRACT: Vaccine therapies based on virus-like particles (VLPs) are currently in the spotlight due to their potential for generating high immunogenic responses while presenting fewer side effects than conventional vaccines. These self-assembled nanostructures resemble the native conformation of the virus but lack genetic material. They are becoming a promising platform for vaccine candidates against several diseases due to the ability of modifying their membrane with antigens from different viruses. The coproduction of extracellular vesicles (EVs) when producing VLPs is a key phenomenon currently still under study. In order to characterize this extracellular environment, a quantitative proteomics approach has been carried out. Three conditions were studied: non-transfected, transfected with an empty plasmid as control, and transfected with a plasmid coding for HIV-1 Gag polyprotein. A shift in EV biogenesis has been detected upon transfection, changing the production from large to small EVs. Another remarkable trait found was the presence of DNA being secreted within vesicles smaller than 200 nm. Studying the protein profile of these biological nanocarriers, it was observed that EVs were reflecting an overall energy homeostasis disruption via mitochondrial protein deregulation. Also, immunomodulatory proteins like ITGB1, ENO3, and PRDX5 were identified and quantified in VLP and EV fractions. These findings provide insight on the nature of the VLP extracellular environment defining the characteristics and protein profile of EVs, with potential to develop new downstream separation strategies or using them as adjuvants in viral therapies.

KEYWORDS: extracellular vesicles, VLP, exosome, vaccine, proteomics



INTRODUCTION

The manufacturing of viral particles for vaccine development is currently an important field of research to explore novel therapies for emerging diseases. Virus-like particles (VLPs) are nanostructures, typically composed of recombinant viral proteins whose outer conformation is identical to the native virus structure but lacking genetic material, hence being noninfectious and thus creating a versatile platform for the generation of vaccines. The recombinant expression of HIV-1 Gag polyprotein in human cell cultures like HEK293 is enough for its self-assembly and release as enveloped VLPs.¹ Gag VLPs are a good platform for the development of vaccines for several diseases. These structures can be used as a scaffold to add immunogenic epitopes decorating its cell membrane, what is known as pseudotyping.² Another important fact in the production of VLPs is the coproduction of extracellular vesicles (EVs), naturally secreted by cell cultures. EVs are cell-membrane-derived nanovesicles that have recently become a major target of research due to their hitherto unknown extent of implication in many diseases.^{3–6} EVs are a heterogeneous population of vesicles produced by all cell types⁷ to deliver cargos, send signals, excrete harmful materials, maintain

homeostasis and regulate many biological processes.^{8–11} This phenomenon can be regarded as a way of cell-to-cell communication.^{12,13} When EVs are produced, they leave the cell, taking part of its membrane, similar to Gag VLPs. When reaching the recipient cell, both cell membranes fuse, the contents of the vesicle enter the cytosol and the membrane of the vesicle becomes part of the recipient cell membrane. Through this process, cells can exchange all sorts of biomolecules such as DNA, RNA, transcription factors, transport proteins, tetraspanins, heat shock proteins, lipid-associated proteins, cytokines, metabolic enzymes, etc.^{7,14,15} It is widely reported that different kinds of EVs are used by the cell for different purposes.^{16,17} An efficient separation of EVs from VLPs is required to obtain high-purity VLP preparations. However, both VLPs and EVs are membrane-bound nano-

Special Issue: Proteomics in Pandemic Disease

Received: July 28, 2020

Published: September 25, 2020



particles sharing the same physicochemical properties, including density and displaying the same families of membrane proteins,^{18–20} which makes strongly difficult their separation. Rounds of centrifugation and density gradients are the current methods for VLP and EV separation but still do not reach good enough purity for vaccine standards.¹⁸ Up to now, there has been no previous work on the molecular characterization of the EV subpopulations copurified with VLPs. Characterizing the protein profile of these EV subpopulations will help cast some light on potential separation approaches. Apart from helping develop a strategy for EV separation, VLP-like EVs could be used as an adjuvant, modifying the membrane composition to promote an immunogenic response or even presenting new antigens via membrane engineering. Furthermore, these EVs could be used as nanocages for drug delivery via metabolic engineering. In this work, a proteomic approach was used to analyze the copurified subpopulations of EVs when producing VLPs and characterize the protein profiles as well as the changes in EV generation when comparing non-transfected and transfected conditions in order to understand the cellular reaction to the production of VLPs regarding EVs.

■ EXPERIMENTAL SECTION

HEK 293 Mammalian Cell Line, Culture Conditions

The cell line used in this work is a serum-free suspension-adapted HEK 293 cell line (HEK293SF-3F6, NRC, Canada) kindly provided by Dr. Amine Kamen from McGill University (Montreal, Canada). Cells were cultured in disposable polycarbonate 125 mL flasks with a vent cap (Corning) at 37 °C, 5% of CO₂, and 85% RH at 130 rpm in a LT-X Kuhner shaker (LT-X Kuhner, Birsfelden, Switzerland). The culture medium was FreeStyle F17 Expression Medium (Gibco, Life Technologies, ThermoFisher, San Jose, CA, USA) supplemented with 8 mM GlutaMAX (Gibco, Life Technologies), 0.1% Pluronic F-68 nonionic surfactant (Gibco, Life Technologies), and IGF-1 at a final concentration of 50 µg/L.

The cell concentration and viability were determined using the NucleoCounterNC-3000 automatic cell counter (Chemometec, Allerød, Denmark) according to the manufacturer's instructions.

Transient Transfection

Transfections were carried out at a cell density of 2×10^6 cells/mL using a final DNA concentration of 1 µg/mL. PEI/DNA complexes were formed by adding PEI to plasmid DNA diluted in fresh culture medium (10% of the total culture volume to be transfected). The transfection reagent PEIpro (Polyplus-transfection, Illkirch-Graffenstaden, France) was used.

The plasmid used contained a gene coding for HIV-Gag protein fused to eGFP (Gag::eGFP). Briefly, pGag::eGFP plasmid is diluted with supplemented FreeStyle F17 medium and vortexed for 10 s.

As a transfection control, a plasmid sharing the same backbone but lacking the Gag::eGFP gene was used and noted as mock. PEI is added in 1:2 (w/w) DNA:PEI ratio and vortexed three times; then, the mixture is incubated for 15 min at room temperature and added to the cell culture.

Ultracentrifugation

VLP containing supernatants were recovered by cell culture centrifugation at $1000 \times g$ for 5 min. Then, concentrated and

purified HIV-1 Gag VLPs were obtained by double cushion ultracentrifugation. Briefly, a volume of 15 mL of clarified supernatant from every condition was layered on top of a 25% (w/v) sucrose cushion (5 mL) and 60% (w/v) sucrose cushion (8 mL) and centrifuged at 31,000 rpm for 2.5 h at 4 °C using a SW32 rotor in a Beckman Optima L100XP centrifuge. Ultracentrifuge tubes were filled with PBS (Hyclone, GE HealthCare, Chicago, IL, USA). The 25–60% sucrose interphase was extracted for each condition. The concentrated material was stored at –80 °C for future studies.

HIV-1 GAG VLP Quantification

The concentration of HIV-1 Gag VLPs was assessed by fluorimetry using a developed and validated quantification assay.²¹ VLP containing supernatants were recovered by cell culture centrifugation at $1000 \times g$ for 5 min. Relative fluorescence unit (RFU) values were calculated by subtracting fluorescence unit (FU) values of non-transfected negative control samples. There is a linear correlation between fluorescence intensity and p24 values determined using the INNOTEST ELISA HIV antigen mAb (Innogenetics NV, Gent, Belgium). RFU values can be converted to Gag::eGFP concentration values using the following equation

$$\text{Gag::eGFP} \left(\frac{\text{ng}}{\text{mL}} \right) = (3.245 \cdot \text{RFU} - 1.6833) \cdot 36 \quad (1)$$

where Gag::eGFP is the estimated concentration of polyprotein and RFU is the measured GFP fluorescence intensity in the samples. The first term is the correlation equation between fluorescence values and p24 concentrations determined by ELISA, and 36 is a correction factor that takes into account the difference in molecular weight between p24 and Gag::eGFP and an underestimation arising from using the p24 ELISA to estimate Gag concentrations. Assuming that a single VLP contains 2500 Gag::eGFP molecules²² and that one Gag::eGFP is 84 kDa (1.39×10^{-10} ng), the concentration of VLPs can be calculated.

Protein Sample Preparation for Mass Spectrometry Analyses

Protein extraction was performed from ultracentrifuged supernatants using extraction buffer (100 mM Tris–HCl pH 8.8, 2 mM EDTA, 4% SDS, 50 mM DTT) from which 100 µL was added to the sample of each condition. Samples were sonicated for 5 min and then boiled for another 5 min. Protein extracts were quantified with an RC/DC Protein Assay (Bio-Rad, Hercules, CA, USA) and stored at –20 °C until the tryptic digestion process. Protein digestion was performed as previously described.²³ Briefly, proteins were digested using sequencing grade trypsin (Promega, Madison, WI, USA) and the filter-assisted sample preparation technology (FASP, Expediton, San Diego, CA, USA), and the resulting peptides were subjected to TMT-10 plex labeling (AB Sciex, Framingham, MA, USA), joined, and desalted. A total of 150 µg of protein from samples of each condition was diluted to a final concentration of 100 mM TEAB labeled with TMT-10 plex according to the manufacturer. Protein samples were labeled by adding 41 µL of TMT isobaric tag diluted in anhydrous acetonitrile, followed by a 1 h incubation step at room temperature. To quench the reaction, 5% (v/v) hydroxylamine (8 µL/sample) was added, incubated for 15 min at room temperature, and mixed together followed by addition of TFA 1% to lower pH at 3. TMT-labeled samples

were equally mixed. Pooled mix was purified using an Oasis HLB C18 column (Waters, Milford, MA, USA).

TMT-labeled peptides were fractionated using a high-pH reversed-phase peptide fractionation kit (Thermo Scientific, San Jose, CA, USA) according to the manufacturer's instructions into five fractions for further LC-MS/MS analysis.

Liquid Chromatography Tandem Mass Spectrometry Analyses

The tryptic peptide mixtures were subjected to LC-MS/MS analysis on a nano-HPLC Easy nLC 1000 liquid chromatograph (Thermo Scientific) coupled to a QExactive mass spectrometer (Thermo Scientific). Peptides were suspended in 0.1% formic acid, loaded onto a C18 reverse-phase trapping column (Acclaim PepMap100, 75 μm internal diameter, 3 μm particle size, and 2 cm length, Thermo Scientific), and separated on an analytical C18 nanocolumn (EASY-Spray column PepMap RSLC C18, 75 μm internal diameter, 3 mm particle size, and 50 cm length, Thermo Scientific) in a continuous gradient (8–31% B in 240 min, 31–90% B in 2 min, 90% B in 7 min, and 2% B in 30 min, where buffer A is 0.1% formic acid in HPLC grade H_2O and buffer B is 100% ACN, 0.1% formic acid in HPLC grade H_2O). Spectra were acquired using full ion scan mode over the mass-to-charge (m/z) range 390–1500, and 70,000 FT-resolution was performed on the top 15 ions in each full MS scan along the chromatographic run, using the data-dependent acquisition mode with 45 s dynamic exclusion enabled. HCD fragmentation was performed at 30% of normalized collision energy.

Protein Identification and Quantification

Protein identification was performed over the raw files using the SEQUEST HT algorithm integrated in the Proteome Discoverer 2.1 (Thermo Finnigan, Thermo Scientific). MS/MS scans were matched against a human database (UniProtKB/Swiss-Prot 2017_10 Release). The sequence of Gag::eGFP protein was added to the selected database to enable identification.

For database searching, parameters were selected as follows: trypsin digestion with 2 maximum missed cleavages allowed, precursor mass tolerance of 800 ppm, fragment mass tolerance of 0.02 Da. TMT-10 plex labeling at the N-terminal and lysine (+229.62932 Da) as well as cysteine carbamidomethylation (+57.021 Da) were chosen as static modifications, whereas methionine oxidation (+15.994915 Da) was chosen as dynamic modification. The same MS/MS spectra collections were searched against an inverted database constructed from the same target database. SEQUEST results were analyzed by the probability ratio method.²⁴ The false discovery rate (FDR) for identified peptides was calculated in the inverted database search results using the refined method.²⁵

TMT reporter ion intensities were extracted from MS/MS spectra for relative quantification of protein abundance to characterize dynamic protein expression profiles in the selected conditions.

Statistical Analysis

For the comparative analysis of the protein abundance changes, we applied the weighted scan peptide–protein (WSPP) statistical workflow,²⁶ using the SanXoT package.²⁷ It uses as an input a list of quantifications in the form of \log_2 ratios (for example, a condition versus control sample) with their statistical weights and generates the standardized forms of

the original variables computing the quantitative values expressed in units of standard deviation around the averages. The quantitative information is obtained from the spectra and used to quantify the peptides from which the spectra are produced and, then, proteins that generate these peptides. In other words, the quantitative information is integrated from the spectrum level to the peptide level and then from the peptide level to the protein level.²⁸ These standardized variables (Z_q) express the quantitative values in units of standard deviation.²⁹ For the protein functional analysis, the Systems Biology Triangle (SBT) model³⁰ was used. This algorithm estimates weighted functional category averages (Z_c) from the protein values by performing the protein to category integration. After the integration from spectra to peptide and peptide to protein, this integration represents a higher level, from protein to category.

The integration allows the detection of changes in functional categories produced by the coordinated behavior of their proteins.²⁸ Together with each Z_q and Z_c , the corresponding FDR was calculated. 5% FDR was considered significant. The quantified proteins were functionally annotated using the Gene Ontology database.^{31,32} For further Gene Ontology annotation, DAVID^{33,34} was used to perform functional enrichment analysis and to extract Benjamini–Hochberg (BH) adjusted p -values for the enriched processes. To help analyze and comprehend the data, the online software REACTOME³⁵ for reaction, protein, and pathway analysis was used.

Interaction Analysis

Proteins identified in the study and described in the online database Vesiclepedia were first subjected to an enrichment analysis using the DAVID bioinformatic tool.^{34,36} Based on their main biological process GO term, five different groups of proteins were selected for further analysis: viral processes, vesicle transport, immune response, DNA and RNA, and cellular response. Each group then followed a protein–protein interaction network analysis using the STRING database.³⁷ The interaction networks and clusters resulting from STRING were edited with the software Cytoscape.³⁸

Particle Size Measurement

Dynamic light scattering (DLS) experiments were performed using a Zetasizer Nano ZS instrument (Malvern instruments, Malvern, UK) with a He/Ne 633 nm laser at 173°. The hydrodynamic diameter, particle size distribution in volume, derived count rate (dCR), and polydispersity index (PDI) were calculated with cumulative fit correlation at 25 °C and 0.887 or 2.448 cP for concentrated samples by ultracentrifugation, respectively. Briefly, 50 μL of sample was placed in disposable plastic cuvettes (UV-Cuvette micro, BRAND GMBH, Germany) followed by automated experimental data collection. Technical triplicates with 12 scans of 10 s were performed in each independent measurement.

Nanoparticle tracking analysis (NTA) was performed with a NanoSight LM20 device (NanoSight Ltd., Amesbury, UK) equipped with a blue laser module (488 nm) to quantify HIV-1 Gag-GFP VLPs and a neutral density filter for total particle by light scattering. Data were analyzed with NanoSight NTA 3.2 software. Briefly, samples were injected, and three technical replicate analyses were carried out. Three video recordings of 60 s length were made for each sample. Subsequently, particles were identified and tracked by their Brownian motion at room temperature. Capture settings were recorded with an sCMOS camera (camera level of 8 for Gag::eGFP VLP samples and 11

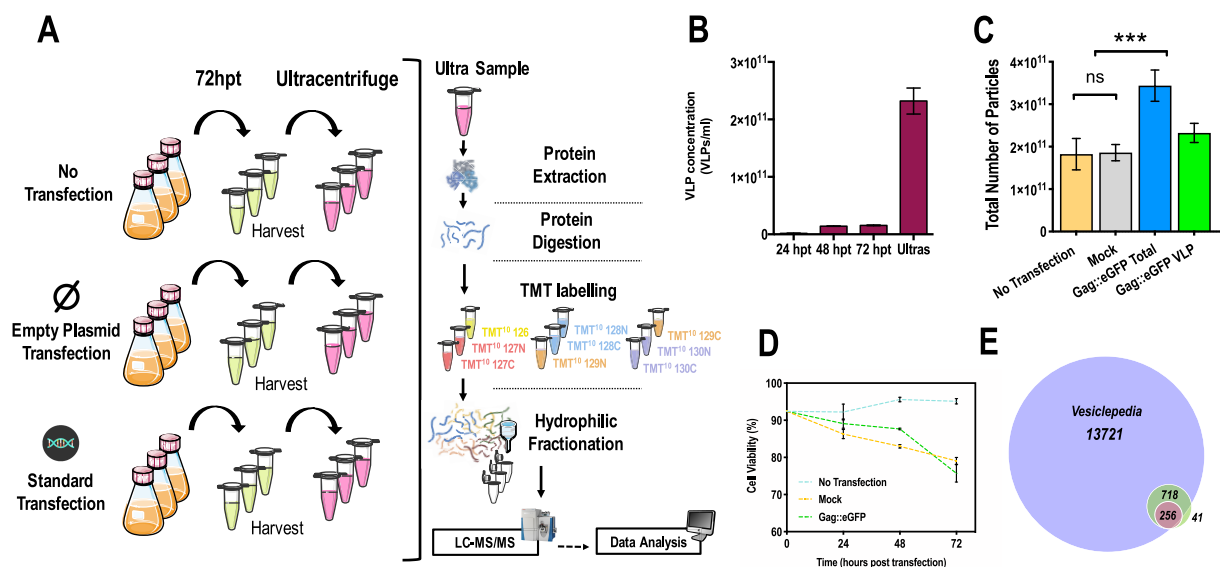


Figure 1. Experimental design and particle production characterization. (A) Proteomic experimental workflow. Three biological replicates of HEK293 cells were cultured in three different conditions. No transfected condition (N), transfected with an empty plasmid denoted as “mock” (M), and transfected using the standard protocol with the plasmid containing the gene gag::egfp (S). At 72 h post transfection (hpt), sample was taken from each replicate and centrifuged at $1000 \times g$ and the pellet was discarded. The stored supernatant was ultracentrifuged at $31000 \times g$ using a sucrose double cushion. The interphase containing VLPs and extracellular vesicles of the same density was extracted. Proteins were extracted from the ultracentrifugation samples and digested, and peptides were labeled using tandem mass tag (TMT) labeling. Labeled peptides were fractionated and analyzed via LC-MS/MS. (B) VLP concentration in the supernatants of the standard transfection condition in the samples before and after ultracentrifugation. (C) Total number of particles measured by NTA in the three different conditions. For the condition transfected with gag::egfp, fluorescent particles were also quantified. Significance calculated using one-way ANOVA, $F = 18.82$, $DF = 8$, and $n = 3$ for each condition. (D) Cell viability throughout the time course of the three different conditions. (E) Venn diagram for the total number of quantified proteins (718) and the number of proteins quantified with more than 1 peptide (256) within the reported proteins in the Vesiclepedia database (13721). There is a total of 41 identified proteins not found in Vesiclepedia from which 33 were identified only with 1 peptide.

for controls, viscosity of 0.9 cP) and analyzed with a detection threshold of 4.

Cryo-Transmission Electron Microscopy (Cryo-TEM)

A 2–3 μL amount of sample was blotted onto holey carbon grids (Quantifoil Micro Tools, Großlobichau, Germany and Micro to Nano, Haarlem, Netherlands) previously glow discharged in a PELCO easiGlow glow discharger unit. The samples were subsequently plunged into liquid ethane at $-180 \text{ }^\circ\text{C}$ using a Leica EM GP cryo workstation and observed in a JEM-2011 electron microscope (JEOL Ltd., Tokyo, Japan) operating at 200 kV. During imaging, samples were maintained at $-173 \text{ }^\circ\text{C}$, and pictures were taken using a CCD-multiscan camera (Gatan Inc., Pleasanton, CA, USA).

Flow Virometry

Flow virometry experiments were performed with a CytoFLEX LX (Beckman Coulter Inc., Brea, CA, USA) with a Violet SSC (VSSC) 405 nm filter, as reported previously.³⁹ The instrument was standardized using Megamix-Plus SSC and FSC fluorescent polystyrene beads (0.1, 0.16, 0.20, 0.24, and 0.5 μm ; Biocytex, Marseille, France) as a quality control tool. The threshold of the trigger signal (VSSC) was manually adjusted to 1500, and gains were set as 95, 9, and 115 for FSC, VSSC, and B525-FITC lasers, respectively. Samples were diluted with PBS 1 \times until an abort rate value below 2%. A total of 300,000 events were analyzed at a flow rate of 10 $\mu\text{L}/\text{min}$ per sample. VSSC-H vs B525-FITC density plots were used to gate the different particle populations (i.e., small EVs, large EVs, fluorescent particles, and HIV-1 Gag::eGFP VLPs). Gating was adjusted manually for each channel. Events after 50 s were taken for analysis. The results were analyzed with

CytExpert software (Beckman Coulter, Brea, CA, USA). Quantitative values were calculated with eq 1:

$$\text{Particle concentration} \left(\frac{\text{Events}}{\text{mL}} \right) = (\text{Events}) \cdot \frac{\mu\text{L}}{\text{mL}} \cdot \text{Dilution} \quad (2)$$

Nuclease and RNase Assay

Absorbance was measured at 260 nm using a NanoDrop 1000 Spectrophotometer (ThermoFisher, San Jose, CA, USA) of samples from non-transfected, transfected with mock, and following the standard transfection protocol conditions. Then, 100 μL of each biological replicate sample was treated with benzonase nuclease (Millipore, Merck, Burlington, MA, USA) diluted in 100 mM Tris-HCl, 20 mM Mg_2Cl at pH 8 and a final concentration of 30 U/mL. After 30 min of incubation at $37 \text{ }^\circ\text{C}$ and gentle shaking, absorbance was measured again at 260 nm. Three technical replicates were measured for each sample. For the RNase assay, vesicle lysis and RNase treatment were performed using a Miniprep Kit (Quiagen, Hilden, Germany) to extract DNA. Lysed samples were again measured at 260 nm.

Western Blots

RC/DC protein quantification was used to normalize protein used for Western blot assay. A total of 35 μg of protein from each condition was separated on SDS-PAGE and transferred onto a polyvinylidene difluoride (PVDF) membrane for 7 min using the system Trans-Blot Turbo Transfer System (Bio-Rad, Hercules, CA, USA) as described in the instructions. Membranes were incubated overnight with diluted primary antibody in 5% (w/v) nonfat dry milk 1 \times TBS 0.1% (v/v)

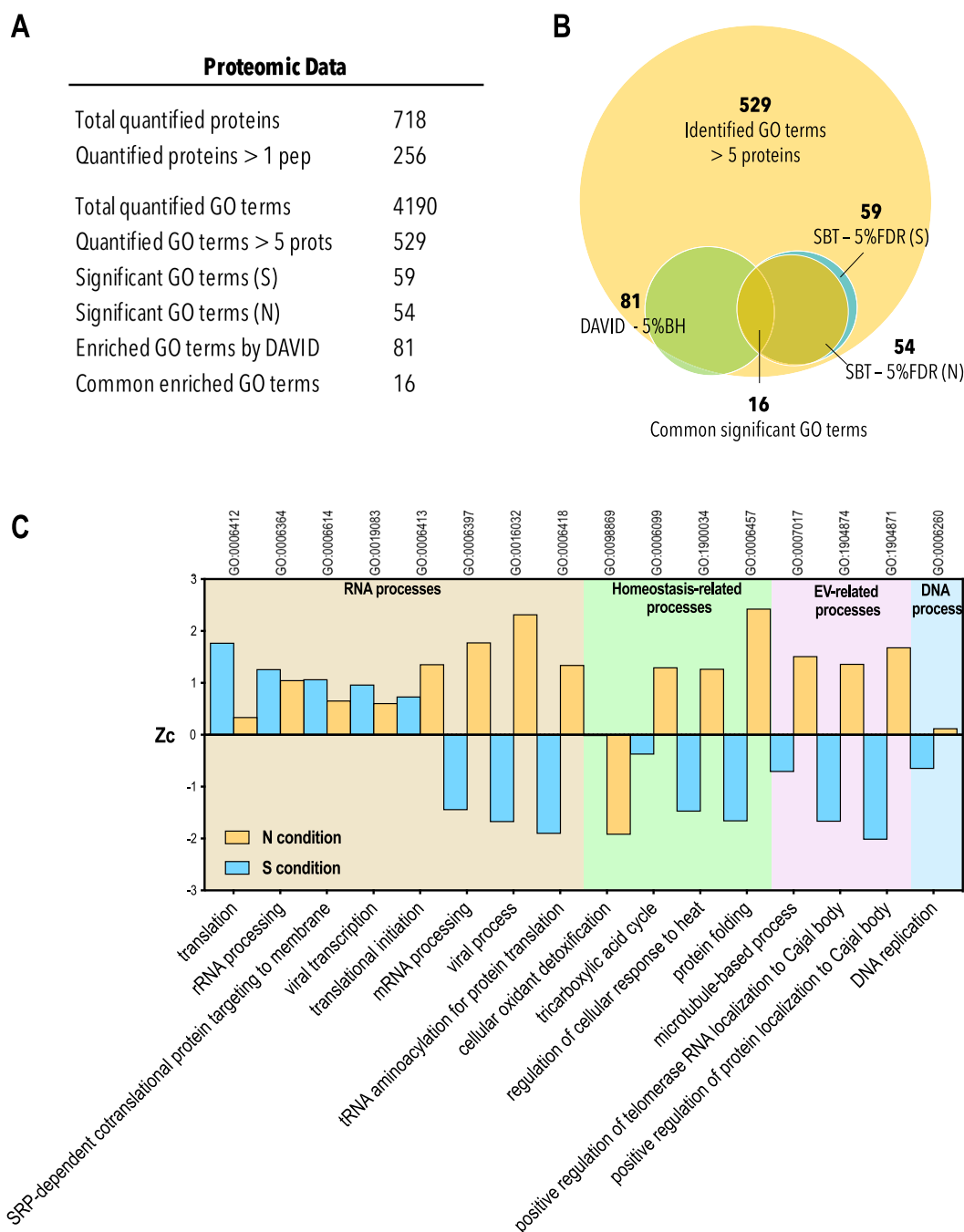


Figure 2. (A) Main proteomic data from the study. Zc values for the S condition were calculated as the ratio of the Zc from standard transfection and mock condition. Zc values for the N condition were calculated as the ratio of the non-transfected and the mock condition. Significant GO terms in the S and N conditions were calculated by the SBT model with 5% FDR. Significant GO terms by DAVID enrichment analysis were calculated using the 256 proteins identified with more than 1 peptide and 5% Benjamini–Hochberg adjusted *p*-value. (B) Venn diagrams showing the main group of analyzed GO terms. The 16 significant common GO terms obtained via DAVID analysis and the SBT model were selected for further analysis. (C) Altered biological processes in VLP-copurified extracellular vesicles at 72 hpt. The X-axis represents the 16 significantly enriched biological process GO terms. 5% BH adjusted *p*-value given by DAVID analysis and 5% FDR by the SBT model. The different Zc values corresponding to each of these GO terms are plotted in the left Y-axis. The yellow series represents the given Zc value for the non-transfected condition, and the blue series, for the standard transfection condition.

Tween-20 at 4 °C with gentle shaking. Primary antibodies used for protein validation were mouse anti-histone H2A antibody (L88A6, Cell Signaling Technology, 1:1000), mouse anti-histone H3 antibody (96C10, Cell Signaling Technology 1:1000), mouse anti-TSG101 antibody (612696, BD Biosciences, 1:1000), mouse anti-ALIX antibody (MCA2493, Bio-Rad, 1:1000), rabbit anti-CD63 antibody (ab134045, Abcam,

UK, 1:1000), mouse anti-CD81 antibody (ab79559, Abcam, UK, 1:1000), and mouse anti-HIV-1 p24 antibody (A2-851-100, Icosagen, Estonia, 1:1000). After primary incubation, a secondary incubation was performed using anti-mouse (A3562, Sigma-Aldrich) or anti-rabbit (A9919, Sigma-Aldrich) antibodies coupled with alkaline phosphatase antibody produced in goat and anti-mouse IgG coupled with alkaline phosphatase

antibody produced in goat as required in 2.5% (w/v) nonfat dry milk $1\times$ TBS 0.1% (v/v) Tween-20 for 1 h at room temperature. Proteins were visualized using NBT-BCIP solution (Sigma-Aldrich) incubating the membrane for 2–3 min. Membranes were let to dry, scanned at 400 bpi, and then analyzed using ImageJ software.⁴⁰

Experimental Design and Statistical Rationale

For the multiplexed quantitative proteomics experiment based on TMT-10 plex labeling, three conditions were tested, with three biological replicates (independent cell cultures) from each: no transfection, transfection of empty mock plasmid, and transfection with the plasmid coding for Gag::eGFP protein following the standard protocol previously described. Samples of each condition were taken at 72 h post-transfection (hpt) followed by an ultracentrifugation to purify HIV-1 Gag VLPs and extracellular vesicles (EVs) with the same density. As is depicted in Figure 1A, the TMT-based isobaric labeling quantification was performed with the three biological replicates for each condition. Protein Zq values comparing the standard transfection vs mock condition were notated as “S condition”. Protein Zq values comparing the non-transfected vs mock condition were notated as “N condition”.

RESULTS

HEK293 VLP Production Analysis

Cell cultures for the standard transfection condition were transfected with a plasmid coding for HIV-1 Gag polyprotein fused to GFP (Gag::eGFP), while mock transfection with an empty plasmid served as a transfection control. An extra condition including non-transfected cells was added to characterize the basal EV production. All transfections were carried out at 2×10^6 cells/mL, and supernatants from all three conditions were harvested at 72 h post-transfection (72 hpt). NTA quantification of fluorescent Gag::eGFP VLPs was used to assess the purification efficiency. Virus-like particles (VLPs) were concentrated around 15 times from $(1.5\pm 0.1)\times 10^{10}$ to $(2.3\pm 0.4)\times 10^{11}$ VLPs/mL (Figure 1B) upon ultracentrifugation. The same purification protocol was carried out with the rest of the samples, and henceforth, all of the analyses are referred to the purified samples. The total number of diffracting particles was assessed by NTA showing that transfection does not influence EV production, as the total number of particles in non-transfected and mock condition does not present any significant difference (p -value = 0.99), with a mean of $(1.82\pm 0.6)\times 10^{11}$ and $(1.86\pm 0.4)\times 10^{11}$ of total particles, respectively (Figure 1C). Reasonably, upon gag::egfp transfection, the total number of particles significantly increases (p -value = 0.0008), up to $(3.44\pm 0.6)\times 10^{11}$ as VLPs are being produced. Comparison of fluorescent over total diffracting particles revealed that the VLP fraction represented the $(68\pm 4)\%$ of the total number of diffracting particles. Thus, copurified EVs are still present in the ultracentrifugation sample. Due to the previous ultracentrifugation step, only copurified vesicles with a similar density to VLPs are being analyzed. The total number of EVs produced was not assessed in this study.

Proteomic Analysis of the HEK293 Secretome

In order to characterize the changes in EV biogenesis and to understand the pathways involved in this process, a multiplexed quantitative proteomics approach based on TMT-10 plex labeling was used. A total of 718 proteins were identified

in this study at 1% FDR, from which 264 had more than 1 peptide. The list of all identified proteins can be found in Supplementary Table S1. The protein database Vesiclepedia was used to match the identified proteins, containing 256 out of the 264 proteins (Figure 1E).

The following analyses were made using the control condition mock to identify changes in the secretome when producing VLPs via transient transfection and in the non-transfected cultures. The SBT model provides functional category averages (Zc) for each biological process derived from the proteins present in the analysis. The ratio of Zc values from the standard transfection and mock condition is notated as “S condition”. The ratio of Zc values from non-transfected and mock condition is notated as “N condition”. A total of 592 biological process gene ontology (GO) terms were quantified with more than 5 proteins in our study, from which 59 and 54 were significantly altered (5% FDR) in the S condition and N condition, respectively (Figure 2A). Therefore, to delimit and filter the most relevant processes, a complementary enrichment analysis was carried out using DAVID over the 256 proteins identified with more than 1 peptide. From this enrichment analysis, 81 biological process GO terms showed a 5% BH adjusted p -value (Figure 2A). Considering the SBT model and DAVID analysis together, a total of 16 significantly enriched biological process GO terms were significantly up- or downregulated in the extracellular environment by the two different models (Figure 2B). The average Zc values of these 16 enriched biological processes resulting from the SBT model are plotted in Figure 2C. A complete overview of the alterations in EV physiology when producing VLPs in cell cultures can be observed in this plot. RNA processing and protein translation pathways were increased when producing VLPs (S condition). This correlated with the metabolic state of producing cells, which was enhanced for protein production and required more energy for it. Conversely, microtubule-based processes, localization of Cajal bodies, protein folding, and viral process GO terms were downregulated in the S condition. Analyzing closely the proteins that were used to annotate these GO terms by the different enrichment tools from DAVID and STRING databases, it was noticed that the observed downregulation in viral processes in the S condition came from a downregulation in nuclear transport proteins, like NUP155 and NUP160 and importins like IPO7 among others (Supplementary Figure S1). The downregulation in nuclear transport has been reported to be triggered upon transfection, in agreement with these results.⁴¹ Within the proteins annotated in the viral process GO term, those involved in protein translation are upregulated (Supplementary Figure S1). Also, analyzing the localization of the Cajal bodies GO term, common proteins like the chaperonin CCTs, heat shock proteins like HSP90 and HSP70, signaling proteins like PPIA, calnexin, and COPB2 were found in all previously mentioned biological processes. T-Complex chaperonin proteins (CCTs) are involved in actin and tubulin folding⁴² as well as in the BBsome formation.⁴³ The BBsome complex plays a role in microtubule-based intracellular transport and is involved in loading cargo into microvesicles.^{44,45} COPB2 is also involved in intracellular vesicle transport, and calnexin is a ER and microvesicle marker. These findings pointed to the fact that microtubule-based vesicle transport, or microvesicle transport, was downregulated when producing VLPs (S condition). On the contrary, in the N condition, these biological processes were upregulated, showing a shift from non-transfected to

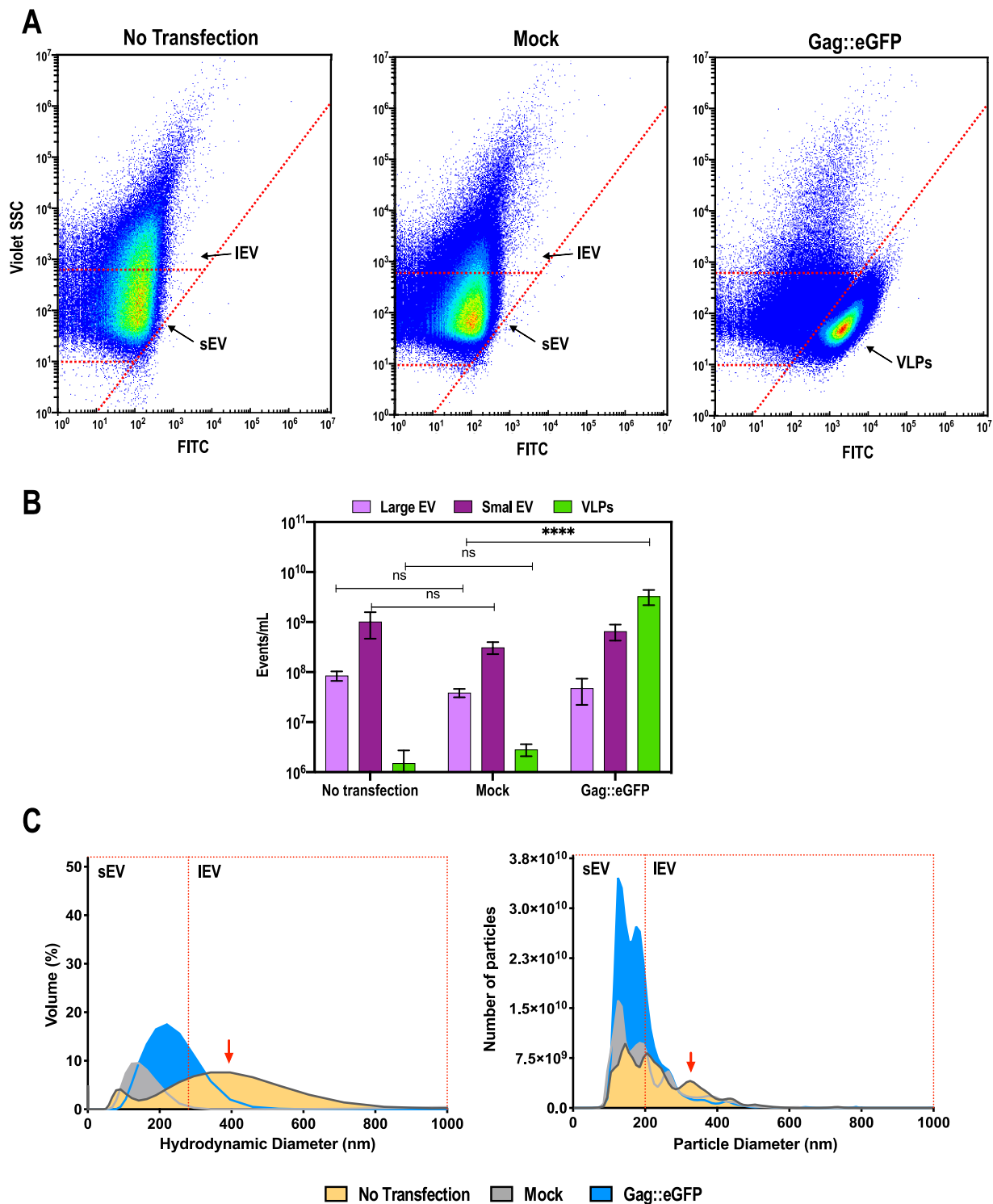


Figure 3. Extracellular vesicle distribution characterization. (A) Flow virometry density plots showing size (violet side scatter) and green fluorescence (FITC) in the three different studied conditions. Different regions correspond to different particle sizes. Regions corresponding to small extracellular vesicles (sEVs) and to large extracellular vesicles (IEVs) are delimited. In the standard transfection condition, the population of green fluorescent particles corresponds to Gag::eGFP VLPs. (B) Quantification of flow virometry subpopulations of large EV, small EV, and VLPs in each of the studied conditions. Significance is calculated via two-way ANOVA, DF = 18. (C) Relative quantification of particles measured by DLS (% of sample volume). Absolute quantification of particles measured by NTA. Red arrows point to the population of large extracellular vesicles.

VLP-producing in microtubule-based vesicle transport. Oxidative stress-related GO terms, like oxidant detoxification, were downregulated in the N condition compared to the S condition, showing an increase in oxidative stress-related

proteins in the EV environment, reflecting the disruption of homeostasis taking place in the cells when VLP production is engaged. Biological processes related to immune activation like antigen processing and presentation increased in S compared

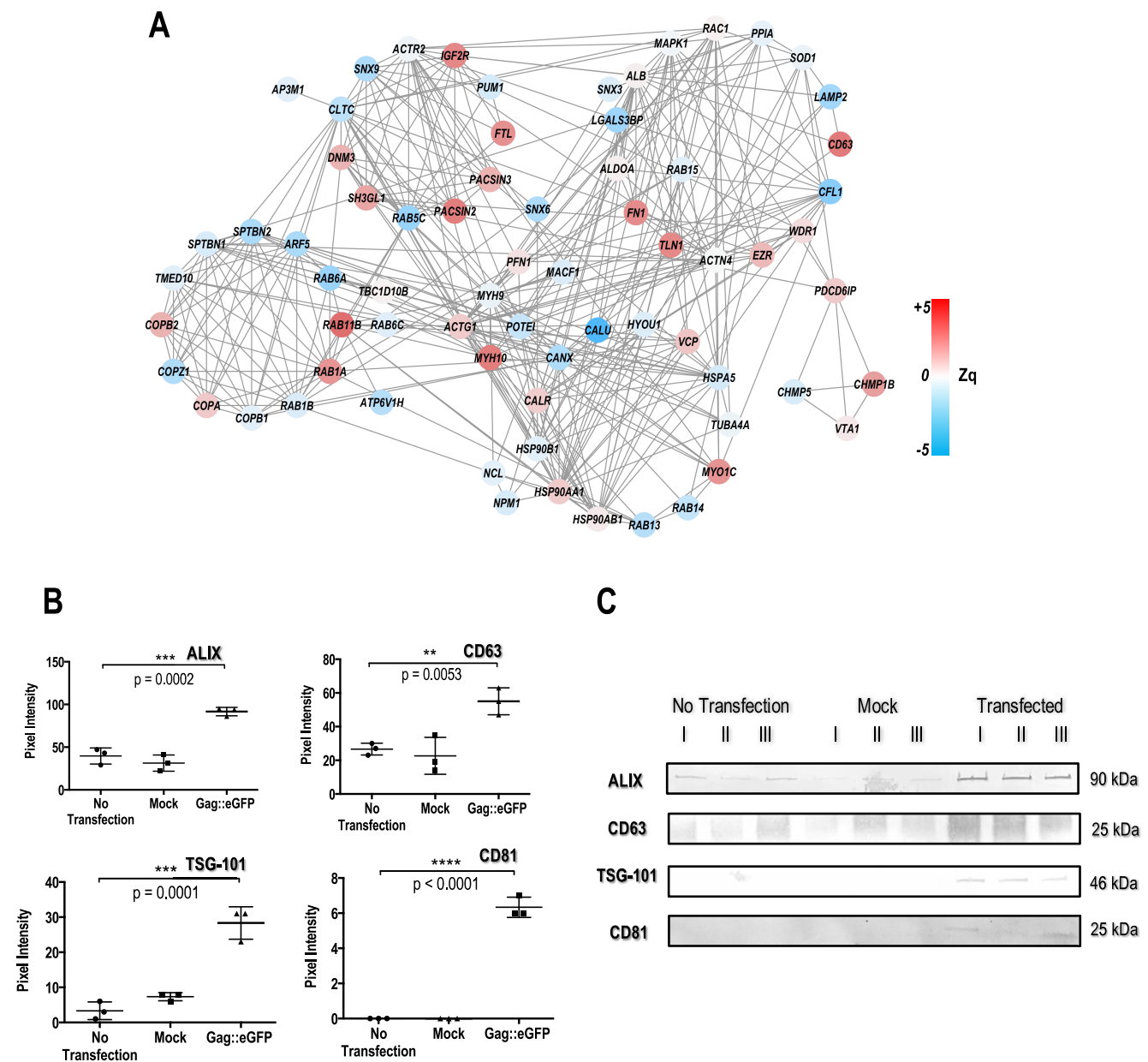


Figure 4. (A) Interaction network of proteins having “vesicle transport” GO annotation and present in Vesiclepedia. Color coding represents the value of Z_q (S condition) of the different proteins in the standard transfection condition. (B) Western blots of non-transfected, transfected with mock, and transfected with gag::egfp conditions. Pixel intensity analysis using ImageJ. Bar plots showing the change in expression of each condition. Medians are represented by horizontal bars, and whiskers extend to extreme data points. p -Values are calculated using one-way ANOVA test, $n = 3$, in each condition: ALIX ($F = 47.16$, $DF = 8$), TSG-101 ($F = 55.97$, $DF = 8$), CD63 ($F = 14.22$, $DF = 8$), CD81 ($F = 361$, $DF = 8$). (C) Western blot membranes. I, II, and III represent the three biological replicates.

to N, suggesting that the proteins present in the cellular membrane of VLPs and vesicles copurified with VLPs have the potential to act as adjuvants in immunization strategies. In addition to this, the DNA replication GO term suggests the presence of histones in the VLP-copurified EVs.

Shift in Extracellular Vesicle Biogenesis: From Large to Small EVs

The total number of particles did not change due to transfection. However, it increased when producing VLPs (Figure 1C). In order to characterize the composition and distribution of particles in each condition, experiments using flow virometry, DLS, and NTA were performed (Figure 3).

Using flow virometry, subpopulations of small EVs (sEVs: 30–200 nm diameter) and large EVs (lEVs: 200–1000 nm diameter) were defined (Figure 3A) using control beads. In the standard transfection condition, a clear subpopulation of GFP positive nanoparticles was observed. This subpopulation was present in the sEV area, suggesting that, indeed, these were VLPs (140–150 nm). Interestingly, although the same total number of particles was measured in the non-transfected and the mock condition, a change in their composition was assessed by this technique. Cytoflex quantification analyses (Figure 3B) proved a significant increase in VLPs in the Gag::eGFP condition. Likewise, the presence of large EVs seemed to decrease when cells were transfected. To confirm

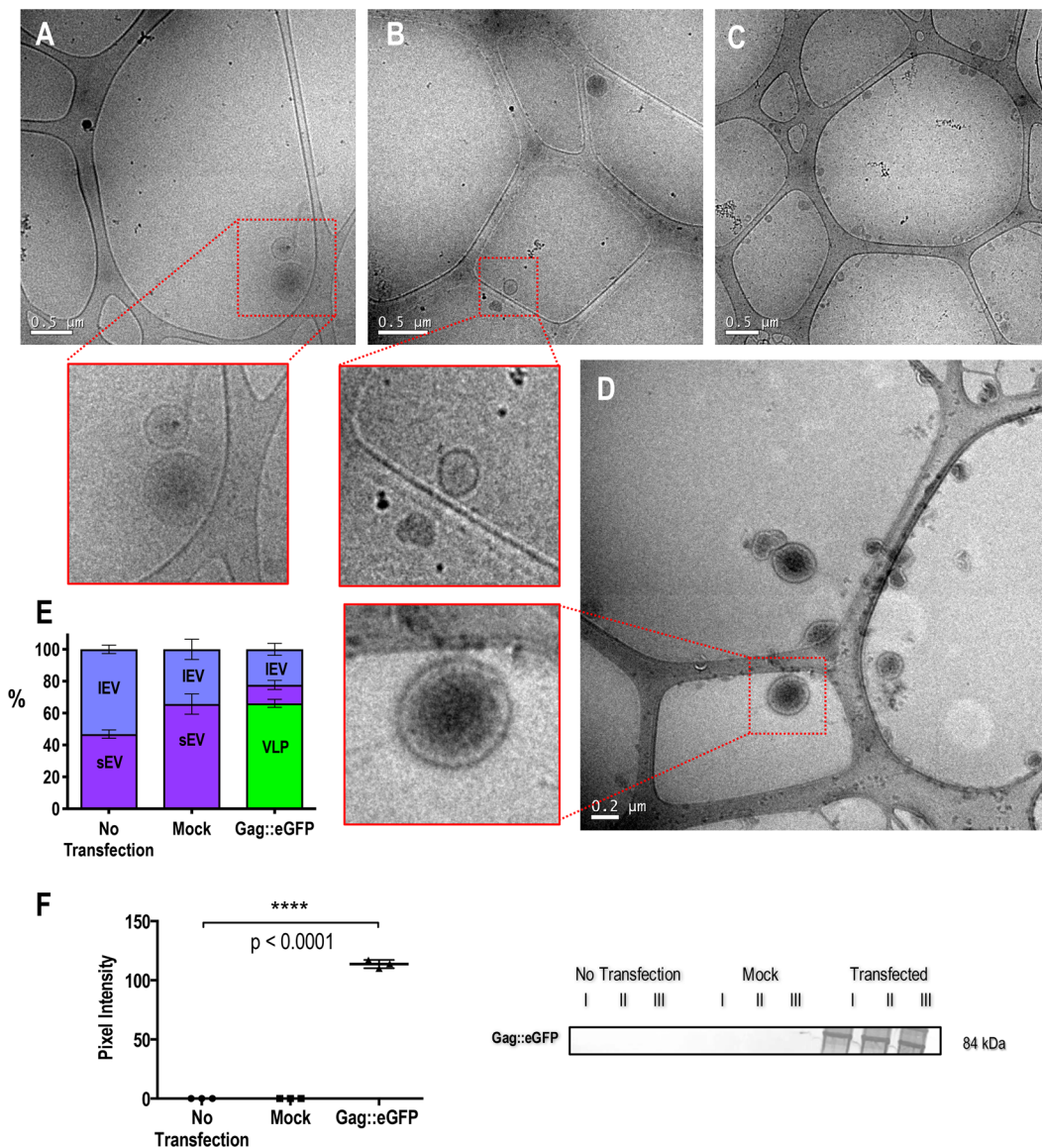


Figure 5. Cryogenic transmission electron microscopy visualization of the vesicle distribution depending of the studied condition. (A) No transfected. The zoomed area depicts a microvesicle, with a diameter larger than 200 nm. (B) Mock. The zoomed area depicts an exosome, with a diameter smaller than 200 nm. (C) Standard transfection. (D) Standard transfection. The zoomed area depicts a VLP, more electrodense than exosomes. (E) Distribution of small EV (sEV), large EV (IEV), and virus-like particles (VLPs) in each condition based on absolute quantification performed by NTA. (F) Western blot of p24 protein, present only in standard transfected condition. The results from these blots were analyzed using ImageJ. *p*-Values of the bar plot showing the change in expression were calculated using one-way ANOVA test, $n = 3$, in each condition, $F = 3143$, $DF = 8$.

the increase in sEVs and the decrease of IEVs, the particle distribution in DLS and NTA was analyzed (Figure 3C). Here, a subpopulation of large EVs of 350–400 nm diameter clearly appeared in the N condition. Likening this condition to the ones which underwent transfection, this large EV subpopulation was no longer observed. However, an increase in sEVs was definitely noted in the mock and standard transfection conditions. In both conditions, two main sEV subpopulations whose diameter was around 140 and 180 nm were highlighted. Consistently, the condition producing VLPs presented a total number of particles which almost doubled the one in the mock condition, in absolute number of particles and also in percentage of total volume, measured by NTA and DLS, respectively. Therefore, taking into consideration that EVs and

VLPs shared the same density, these findings suggested a shift in EV biogenesis upon transfection, from larger to smaller EVs.

In order to characterize this shift in vesicle biogenesis, proteins involved in microvesicle (MV), exosome biogenesis, and vesicle-transport-related processes were analyzed. As previously observed in Figure 2, the main GO analysis revealed that microvesicle-mediated transport was downregulated in S. For a deeper study of the proteins involved, an interaction network analysis using STRING was carried out for the proteins associated with the vesicle-transport biological function GO term. The interaction network resulting from this analysis is shown in Figure 4A, whose Zq value corresponded to standard transfection vs mock condition. Here, it was observed that proteins involved in MV budding like ARF5 or AP3M1 were downregulated in the standard

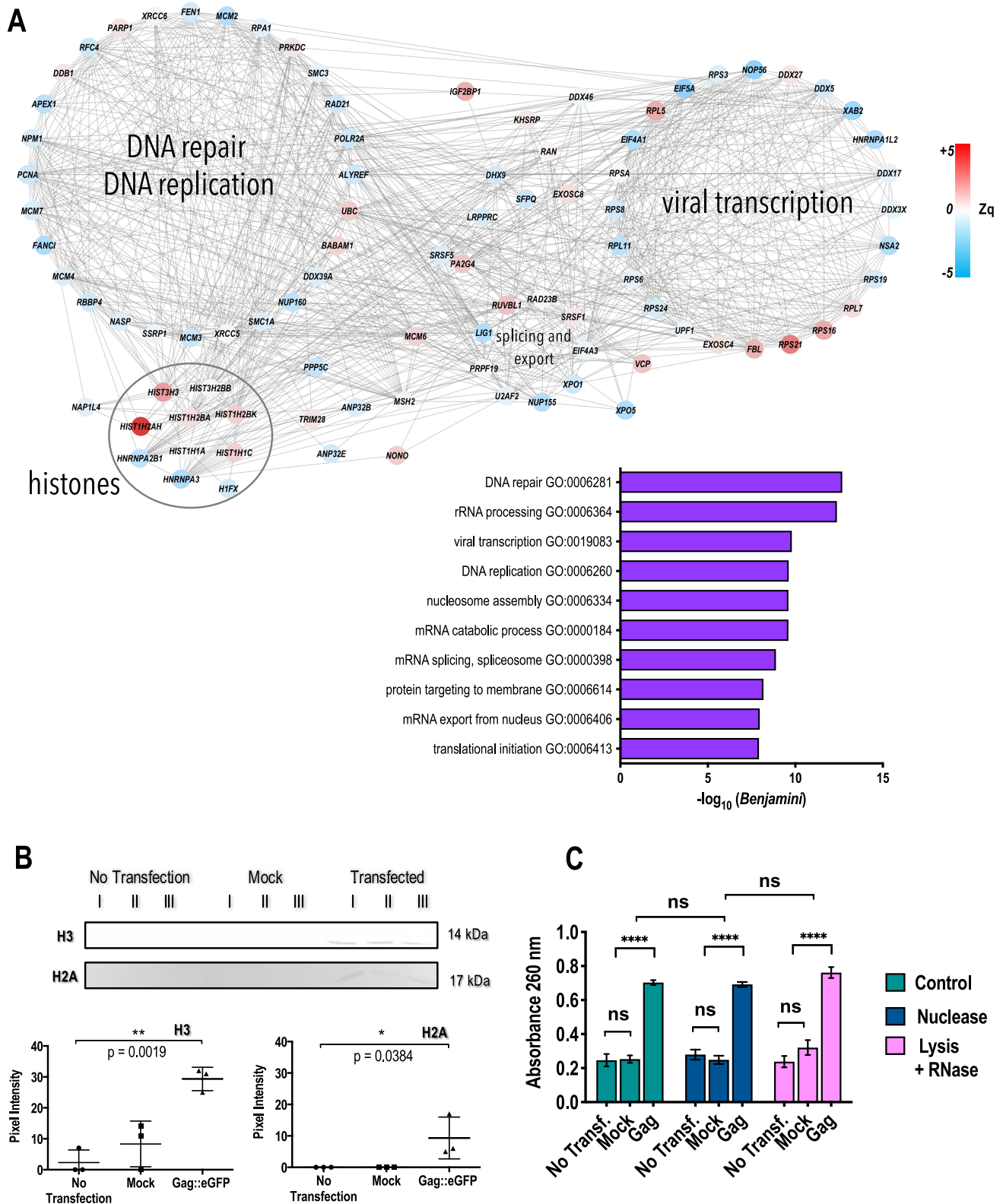


Figure 6. DNA- and RNA-associated protein analyses. (A) Interaction network of proteins having DNA- and RNA-related GO annotation and present in Vesiclepedia. Color coding represents the value of Z_q (S condition) of the different proteins in the standard transfection condition. Labeling for the different clusters represents the enriched GO term corresponding to the proteins present in the cluster. The top 10 enriched GO terms and their corresponding Benjamini p -value from the group of proteins annotated with DNA- and RNA-related biological functions are presented in the bar chart. (B) Western blots of non-transfected, transfected with mock, and transfected with gag::egfp conditions for H3 and H2A proteins. The results from these blots were analyzed using ImageJ. Bar plots showing the change in expression of each condition. Medians are represented by horizontal bars and whiskers that extend to extreme data points. p -values are calculated using one-way ANOVA test, $n = 3$, in each

Figure 6. continued

condition H3 ($F = 21.28$, $DF = 8$), H2A ($F = 5.895$, $DF = 8$). (C) Nuclease and RNase assays. Absorbance at 260 nm was measured before any treatment (control), after a nuclease, and after lysis and RNase treatment. Significance is calculated using two-way ANOVA test, $DF = 18$.

transfection condition. Other downregulated proteins like CFL1, SPTBN1, and SPTBN2 are involved in cytokinesis and cytoskeleton-related contraction processes, promoting MV budding. MV biomarkers like CANX were also downregulated. On the other hand, proteins involved in the formation of the late endosomal compartment or MVB and its later fusion to the cell membrane were upregulated in the S condition. Proteins involved in endocytosis like PACSIN2, SH3GL1, IGF2R, RAB11, RAB1A, and DNMT3 were increased in S, suggesting that the MVB pathway for production of exosomes was upregulated, coinciding with the increase in the sEV fraction observed by DLS and NTA. On top of that, proteins reported to be exosome biomarkers were found to be upregulated, like FN1, TLN1, FTL, CD63, and some components of the ESCRT complexes, like CHMPB1, PDC6CI (ALIX), and TSG-101 (Figure 4B,C). The protein interaction analysis supported that there was a shift from IEV biogenesis to the upregulation of the MVB pathway, producing sEVs in mock and standard transfection conditions. When visualizing a total of 176 particles using cryogenic transmission electron microscopy, in non-transfected samples, vesicles larger than 200 nm were found (Figure 5A). In mock and standard transfection conditions (Figure 5B,C), vesicles smaller than 200 nm were observed, and coherently with the increase in particles reported by NTA, the concentration of particles in the standard transfection condition for the same analyzed area was much higher than in the mock condition. Interestingly, VLPs are shown as electrodense particles compared to other EVs. It can be observed that there is a shell of ~ 20 nm that might be corresponding to the Gag::eGFP shell below the plasma membrane. Therefore, it was corroborated that the increase in the number of particles upon transfection was not only due to the increment of electrodense particles (Figure 5D) but also to the increase of non-electrodense particles smaller than 200 nm (sEVs), as shown in Figure 5C, validating the fact that Small EV biogenesis was indeed incremented upon transfection. This shift was also observed analyzing the particle size distribution given by NTA. In non-transfected samples, $(47 \pm 3)\%$ of the total particles were smaller than 200 nm and $(53 \pm 4)\%$ larger than 200 nm. Upon transfection with mock plasmid, these percentages shifted to $(66 \pm 9)\%$ of particles smaller than 200 nm and $(34 \pm 9)\%$ of particles larger than 200 nm (IEVs). This tendency continued when producing Gag::eGFP (Figure 5F), where $(88 \pm 6)\%$ of all particles were under 200 nm, from which $(68 \pm 4)\%$ were fluorescent (VLPs) and the rest were sEVs. Here, only $(22 \pm 6)\%$ were particles above 200 nm, evidencing the shift from IEV to sEV biogenesis (Figure 5E).

The Increase in sEVs Correlates with DNA Secretion

Similarly to the interaction analyses performed for vesicle-transport-related proteins, an interaction analysis of DNA- and RNA-related processes was carried out for the identified proteins. As is observed in Figure 6A, most of the proteins related to DNA and RNA processes were downregulated upon VLP production. These proteins are involved in biological functional processes like DNA replication, DNA repair, and mRNA splicing (Figure 6A). The event of transient transfection substantially impacts intracellular homeostasis, disrupt-

ing then processes such as DNA repair and maintenance. Consequently, a downregulation in these proteins was observed upon transfection and VLP production. Since in the S condition Gag polyprotein was being largely produced, ribosomal proteins like some proteins belonging to the RSP and RLP protein family were upregulated, corresponding to the process of translation initiation.

Nevertheless, the highest upregulation observed in this group of proteins was found for histones. The presence of histones in copurified EVs during VLP production has been reported before.^{46,47} Coherently, histones were upregulated in samples corresponding to the S condition (Figure 6B), suggesting DNA was present inside sEVs or VLPs, since this upregulation in histones was found in the purified samples of EVs and VLPs. DNA can be secreted within these structures, or even owing to the sticky nature of DNA due to its electric charge, it can be adhered to the outside surface. The absorbance at 260 nm was measured in samples from non-transfected, mock, and standard transfection conditions before and after performing a nuclease treatment. This technique was used to remove potential DNA contamination that might be present outside the vesicles and VLPs. Absorbance readings after the assay showed that the nuclease treatment did not reduce the signal at 260 nm. To further assess the DNA presence within these structures and discard that this signal is coming from the RNA presence, a DNA purification protocol was performed, comprising vesicle lysis and RNase treatment. Afterward, absorbance at 260 nm was again measured, showing no significant difference (Figure 6C). Taking into account the particle concentration of each condition, the ratio of absorbance per particle was calculated as 0.13, 0.13, and 0.20 (Abs units/ 10^{11} particles) in non-transfected, mock, and standard transfection conditions, respectively. A significant increase (p -value = 0.0351) was observed in the standard transfection condition. Therefore, it could be concluded that DNA was present inside EV structures and it correlates with the previously observed increase in sEVs. Curiously, in non-transfected samples, there was a basal DNA presence, which might be due to the fact that the cell uses exosomes to excrete harmful DNA.¹⁰ This basal presence, or absorbance at 260 nm, did not increase upon transfection. Mock condition samples showed the same level of DNA presence. However, there was a significant increment of DNA in the VLP production condition, being coherent with the upregulation in histones found in the proteomic analysis. However, the relative contribution of VLPs and other sEVs to the DNA presence remains unclear.

Energy Homeostasis Disruption Is Reflected in EVs

Extracellular vesicles are normally produced as a way of cell-to-cell communication. The contents of these structures reflect the physiological state of the cell generating them. Analyzing the changes in metabolic proteins in EVs, we can get a glimpse of how homeostasis is regulated in every condition.

Protein ubiquitination was upregulated in the S condition. Many of the proteasome subunits were found to be upregulated in EVs upon transfection and VLP production (Figure 7). This suggested that protein degradation was

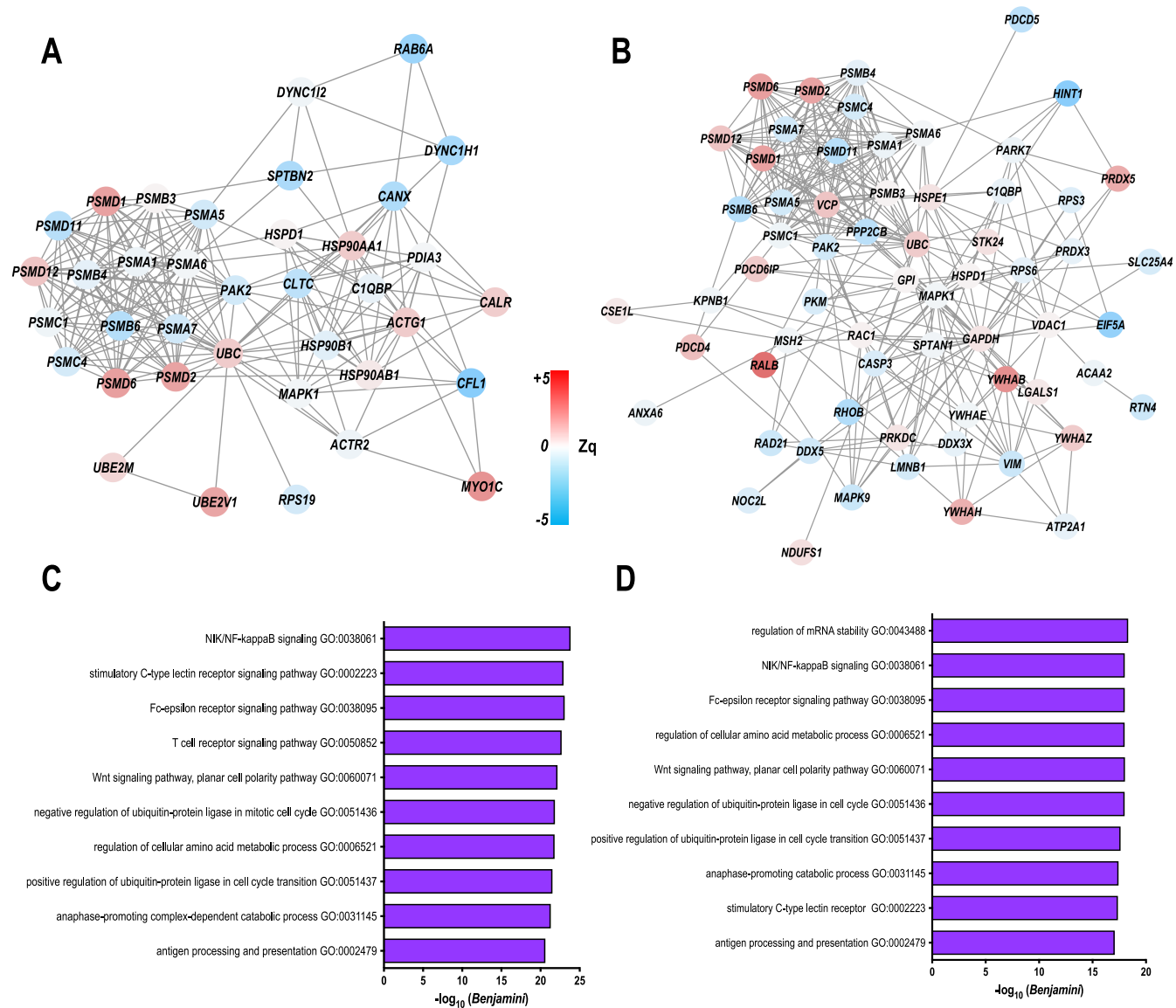


Figure 7. Protein interaction networks corresponding to the immune system process and the cellular response gene ontology annotation. (A) Identified proteins present in Vesiclepedia with immune response GO annotation. (B) Identified proteins present in Vesiclepedia with cellular response GO annotation. Color coding represents the value of Z_q (S condition) of the different proteins in the standard transfection condition. (C) Enrichment analysis of GO terms from the group of proteins annotated with the immune response biological function. (D) Enrichment analysis of GO terms from the group of proteins annotated with the cellular response biological function.

upregulated. The reason triggering this upregulation could be found in the mitochondria. Mitochondrial content was upregulated upon VLP production, creating an increment of ROS that needed to be detoxified. There was an increase in peroxiredoxins, thioredoxins, and other oxidant detoxifiers in the S condition. The increment of mitochondria correlated with an increment in proteins involved in glucose metabolism, reflecting the high energy demand. However, TCA proteins and different ATP-metabolism-related proteins were down-regulated (Figure 2). This evidenced that the cell is communicating energy homeostasis disruption via extracellular vesicles. This energy homeostasis disruption agrees with previously reported results.⁴¹ Apoptotic markers like thrombospondin-2 (THB-2) were found to be upregulated together with proteasome subunits, RALB or PRDX5, also indicating the redox detoxification event (Figure 7B).

Proteins Related to the Immune System Found in Copurified Vesicles

Immune activation, inflammation and oxidative stress response are biological processes influencing the development of an immunogenic response when patients are vaccinated. When producing VLPs, copurified extracellular vesicles and VLPs presented proteins associated with these immune-system-related processes. Proteins like ACTG1, ITGB1, ENO3, PRDX5, GAPDH, YWHAB, RAC1, TXN, HSPA1L, and 10 other proteins from the HSP family are associated with stress response, oxidative stress, and immune system modulation (Figure 7A,B). An enrichment analysis of these proteins showed that they are involved in T cell receptor signaling, stimulation of C-type lectin receptor signaling, and antigen processing and presentation processes among others (Figure 7C,D). These processes have been reported to be stimulated and activated by adjuvants in current vaccine therapies.^{48,49}

DISCUSSION

Extracellular vesicles, including VLPs, are produced by different cellular pathways. Identifying and characterizing how cells behave and modulate EV biogenesis upon transfection can be used to define optimization strategies to enhance VLP production. Depending on the biogenesis pathway used, EVs present different characteristics. Microvesicles (MVs) are particles of 50–2000 nm diameter.⁵⁰ Their size range is so broad that it overlaps with the rest of the EVs. Microvesicles are produced by direct outward budding of the plasma membrane. Contraction of actin and myosin structures helps redistribute the components of the plasma membrane, creating a membrane evagination and thus completing the budding process.⁵¹ These structures present marker proteins like calnexin or ARF5, ARF6^{3,52} and lack others like ALIX or TSG-101, which are highly present in exosomes.⁵³ Exosomes are nanoparticles of 30–100 nm diameter which are produced by different mechanisms, like the multivesicular bodies (MVB)⁵⁴ pathway. Here, cargo is loaded into intracellular endosomal compartments, forming intraluminal vesicles (ILVs).¹⁶ These are invaginations of the membrane toward the lumen of the endosome. The ILVs are ultimately bound by the plasma membrane, but as a result of two invaginations, they are contained within a larger endosome. This late endosome then fuses with the plasma membrane, releasing its contents of ILVs to the extracellular space and becoming exosomes. The cargo present in exosomes can be DNA, RNA, enzymes, cytokines, etc., although many of the mechanisms of loading these cargos are still unknown. On the other hand, the process of budding into the luminal face of the endosome has been well reported. First, microdomains rich in tetraspanins like CD81, CD9, and CD63 seem to play an important role, being the anchoring site for proteins to dock and start the budding process.^{20,55,56} This makes them widely accepted exosome biomarkers. The endosomal sorting complex required for transport (ESCRT) is responsible for loading the cargos and inducing the ILV formation.⁵⁷ Cargos interact with TSG-101 and ALIX, components of complexes ESCRT-I and ESCRT-II, respectively.^{58,59} This promotes the recruitment of the cargo and the components of the ESCRT-III, responsible for excision. HIV-1 virions have been described to bud off directly from the plasma membrane as well as via the MVB pathway.^{60,61} The Trojan exosome hypothesis proposes that HIV uses the existing exosome biogenesis pathway to produce infectious particles.⁶¹ This hypothesis is supported by experiments that showed viral particles presenting exosome biomarkers like tetraspanins CD63, CD81, and CD9⁶² as well as endosome components,⁶³ showing that HIV uses the MVB vesicle production mechanism to bud off from the cell. More evidence backed up this model, as proteins like TSG-101 and ALIX were found in HIV virions.⁶⁴ However, HIV mainly buds off directly from the cell membrane recruiting the ESCRT complexes as well as using the tetraspanin-enriched microdomains of the cell membrane.⁶⁵ Gag polyprotein has been observed to interact with TSG-101, ALIX, tetraspanin-enriched domains, lipid rafts, and other endosome components. This suggests that both pathways are used by the virus to release from the host cell and therefore for VLP production. The results from this work showed that there is a shift from large to small EVs, and based on the protein profile observed, it could be associated with a change from microvesicle to exosome biogenesis in HEK293 upon transfection. This could be due to

the fact that Gag VLPs leave the cell using ESCRT machinery which is present in the MVB pathway as well as in the plasma membrane, reducing cell resources and physical space at the plasma membrane for microvesicle production. The increased recruitment of ESCRT due to the high Gag intracellular concentration might be promoting the exosomes biogenesis pathway, since it is also used for VLP production. The evidence suggesting the increase in intracellular trafficking pathways is crucial to explore the optimization of intracellular Gag VLP production.

Transfection and VLP production generate a state of disrupted energy and redox homeostasis within the cell. The cell communicates this state to its extracellular environment by releasing EVs containing proteins reflecting the disruption. This homeostasis disruption is observed in transfected cultures, where VLP production is enhanced. The uptake of these produced EVs could influence the homeostasis of the recipient cell, promoting VLP production. Once homeostasis is disrupted, the cell tries to excrete harmful material, causing this disruption. Exosomes are the main resource for the cell to secrete unwanted material like harmful proteins that cannot be degraded, foreign DNA, enzymes, etc.¹⁰ This could be another reason for the observed shift from microvesicle to exosome generation. This fact could also explain the presence of DNA within sEVs. It is all triggered by VLP production. Cells have been transfected with large amounts of DNA. Therefore, cells can be using sEVs, including VLPs, to excrete it. Considering a VLP of ~140 nm diameter, with the Gag::eGFP shell being ~20 nm thick according to the cryoelectron micrographs, and considering a nucleosome of 11 × 5.5 nm,⁶⁶ it can also be possible that DNA is secreted together with histones forming nucleosomes within VLPs, as one nucleosome would only represent 0.2% of the available volume. The NC domain of Gag polyprotein is reported to interact with nucleic acids and serve as a scaffold in virion assembly.^{67,68} Lacking viral RNA, host cell DNA might be serving as a scaffold in VLP formation. The NC domain might be the docking point of nucleic acids. Therefore, if a DNA-free vaccine is envisaged, an engineered NC domain, preventing nucleic acids from docking and being incorporated into the VLPs, might be a future study objective.

The presence of EVs has been a topic of interest in many HIV-1 Gag VLP studies.^{39,69–73} They are mostly regarded as contaminants, as the efficiency of VLP production was calculated by the percentage of VLPs achieved in the proposed bioprocess compared to the total number of diffracting particles produced (including EVs). However, their presence in the copurified fraction of the VLPs could be used as an adjuvant for future therapies. The potential use of exosomes conjugated with VLPs and other different nanoparticles as a vaccine is currently being explored, since many cancer treatments have proven to be improved by using exosomes as adjuvants.⁷⁴ Exosomes are considered a key element subject to further study in order to use them as a potential adjuvant for a VLP-based therapy.

The future combined use of VLPs and EVs could offer a new alternative for the further development of a HIV-1 prophylactic vaccine. This is still a major challenge for science nowadays. Several strategies have been developed for a protective HIV-1 vaccine, such as MPER-V3 HIV-1 VLP, modified Vaccinia Ankara (MVA)-based vaccine candidates, or even DNA vaccines.^{75,76} However, none showed significant results in humans. Although eliciting a strong immune response, no strategy was able to generate quality antibodies to achieve

protection. The main limitation hitherto encountered is the selection of the immunogen or antigen which leads to the generation of high-quality neutralizing antibodies. The combined use of EVs offers a new possibility to combine antigens with immunomodulatory proteins to try the generation of a more specific immune response.

Whether EVs are used as adjuvants or considered impurities in VLP-based therapies, methods of separation are required to reach high-purity preparations. The EV characterization performed in this work shows that ultracentrifugation is not enough to fully separate exosomes/microvesicles from VLPs. Chromatography strategies have also been implemented to purify VLPs.⁷⁷ However, the low yields achieved suggest the need for a more specific separation protocol in order to be implemented at large scale. Taking into account the biogenesis pathways of the different EVs copurified with VLPs and the characterization of the defined protein profile, it is possible to design metabolic engineering strategies to further develop a specific downstream process. Affinity chromatography could be designed, and affine proteins could be overexpressed in these vesicles. The actual impossibility to efficiently separate these subpopulations remains one of the main challenges to overcome.

Taking into account the great potential of exosomes to complement the effect of VLPs, the next envisaged step would require vesicle engineering in order to isolate exosomes containing proteins which could contribute to improve the immunogenic response. Proteins promoting oxidative stress protection and anti-inflammatory proteins like ENO3 or PRDX5 could be engineered to be coproduced with VLPs, cotransfecting their coding genes together with *gag::egfp*. Another possibility could be metabolic engineering to neutralize the homeostasis disruption signaling which takes place in the cell cultures when producing VLPs. In order to do that, a further study of the glycome of EVs and VLPs would be required. Apart from modifying the outer layer of the vesicle membrane customizing glycoproteins and specific signaling proteins, another interesting target would be the VLP cargos. Gag polyprotein could be used as the anchor to interact with cargos and load them into the VLPs. RNA is described to interact with Gag and to be necessary as a scaffold for Gag multimerization and further VLP formation.^{67,78,79} This particularity could be used to design miRNAs with protective effects, such as anti-inflammatory or immune activation effects to be loaded to the VLPs. In order to do that, a further study in the selectiveness of Gag for different species of RNA and targeting strategies would be required and should be assessed to successfully develop an effective VLP-based therapy.

CONCLUSIONS

Characterizing the extracellular environment of the produced VLPs is essential in order to design future VLP-based therapies. In this work, a multiplexed quantitative proteomic approach has been used to determine changes taking place in the secretome of VLP-copurified EVs. When producing VLPs, there is a shift from microvesicle to exosome biogenesis, increasing in 30% the production of vesicles smaller than 200 nm. This change comes together with a disruption of energy and redox homeostasis. DNA is secreted in these small EVs, whose presence is increased when producing VLPs. Another remarkable trait of the extracellular environment accompanying VLPs is the presence of immunomodulatory proteins in these vesicles. Proteins associated with immune activation,

anti-inflammatory processes, and response to oxidative stress were identified in this coproduced fraction. The characterization of EVs which copurify with VLPs after a first basic purification step is key to develop further, more specific downstream purification processes or to use these copurified vesicles to our advantage to design exosome-based adjuvants.

ASSOCIATED CONTENT

Supporting Information

The Supporting Information is available free of charge at <https://pubs.acs.org/doi/10.1021/acs.jproteome.0c00581>.

Figure S1: Interaction network of proteins having “viral process” GO annotations and present in Vesiclepedia (PDF)

Table S1: List of all identified proteins in this study (XLSX)

AUTHOR INFORMATION

Corresponding Author

Jesús Lavado-García – *Grup d'Enginyeria Cel·lular i Bioprocés, Escola d'Enginyeria, Universitat Autònoma de Barcelona, 08193 Barcelona, Spain*; orcid.org/0000-0001-9993-6332; Email: jesus.lavado@uab.cat

Authors

Irene González-Domínguez – *Grup d'Enginyeria Cel·lular i Bioprocés, Escola d'Enginyeria, Universitat Autònoma de Barcelona, 08193 Barcelona, Spain*; orcid.org/0000-0002-7920-5505

Laura Cervera – *Grup d'Enginyeria Cel·lular i Bioprocés, Escola d'Enginyeria, Universitat Autònoma de Barcelona, 08193 Barcelona, Spain*

Inmaculada Jorge – *Laboratory of Cardiovascular Proteomics, Centro Nacional Investigaciones Cardiovasculares (CNIC), Madrid 28029, Spain; Centro de Investigación Biomédica en Red Enfermedades Cardiovasculares (CIBERCV), Madrid, Spain*

Jesús Vázquez – *Laboratory of Cardiovascular Proteomics, Centro Nacional Investigaciones Cardiovasculares (CNIC), Madrid 28029, Spain; Centro de Investigación Biomédica en Red Enfermedades Cardiovasculares (CIBERCV), Madrid, Spain*

Francesc Gòdia – *Grup d'Enginyeria Cel·lular i Bioprocés, Escola d'Enginyeria, Universitat Autònoma de Barcelona, 08193 Barcelona, Spain*

Complete contact information is available at: <https://pubs.acs.org/doi/10.1021/acs.jproteome.0c00581>

Author Contributions

J.L.-G. designed and performed experiments, analyzed and interpreted data, and wrote the paper. I.G.-D. contributed with NTA, DLS experiments, and Cytotflex data analysis. L.C. and I.J. supervised and contributed to its analysis and edited the manuscript. J.V. and F.G. supervised and edited the manuscript.

Funding

The project that gave rise to these results received the support of a fellowship from “la Caixa” Foundation (ID 100010434). The fellowship code is LCF/BQ/ES17/11600003. The research group is recognized as 2017 SGR 898 by Generalitat de Catalunya. This study was also supported by competitive

grants from the Spanish Ministry of Science, Innovation and Universities (BIO2015-67580-P and PGC2018-097019-B-I00), through the Carlos III Institute of Health-Fondo de Investigación Sanitaria grant PRB3 (IPT17/0019 - ISCIII-SGEFI/ERDF, ProteoRed), the Fundació MaratóTV3 (grant 122/C/2015), and “la Caixa” Foundation (HR17-00247). The CNIC is supported by the Instituto de Salud Carlos III (ISCIII), the Ministerio de Ciencia e Innovación, and the Pro CNIC Foundation and is a Severo Ochoa Center of Excellence (SEV-2015-0505).

Notes

The authors declare no competing financial interest. The raw mass spectrometry data has been submitted to the ProteomeXchange Consortium (<http://proteomecentral.proteomexchange.org>) with the data set identifier PXD018114.

ACKNOWLEDGMENTS

The authors thank Dr. Amine Kamen (McGill University, Montreal, Canada) for providing the HEK 293 SF-3SF6. The following reagent was obtained through the National Institutes of Health AIDS Reagent Program, Division AIDS, National Institute of Allergy and Infectious Diseases, National Institutes of Health: pGag::eGFP (Cat. No. 11468) from Dr. Marilyn Resh. The support of Dr Jose Amable Bernabé from the Institute of Material Science of Barcelona (ICMAB-CSIC, Barcelona, Spain) with particle tracking techniques and the help of Marti del Cabo from the Microscopy Service from the Autonomous University of Barcelona (Barcelona, Spain) in the performance of electron microscopy analysis are greatly appreciated.

ABBREVIATIONS

BH, Benjamini–Hochberg; DTT, dithiothreitol; EDTA, ethylenediaminetetraacetic acid; eGFP, enhanced green fluorescence protein; ESCRT, endosomal sorting complex required for transport; EVs, extracellular vesicles; F17, FreeStyle F17 cell culture medium; FASP, filter aided sample preparation; Gag::eGFP, translational fusion of HIV-Gag protein and eGFP; hpt, hours post transfection; ILV, intraluminal vesicles; LC-MS, liquid chromatography coupled with tandem mass spectrometry; IEVs, large extracellular vesicles; MVs, microvesicles; MVBs, multivesicular bodies; MVA, Modified Vaccinia Ankara; PBS, phosphate-buffered saline; PEI, polyethylenimine; RFUs, relative fluorescence units; SBT, Systems Biology Triangle; SDS, sodium dodecyl sulfate; sEVs, small extracellular vesicles; TEAB, tetraethylammonium tetrahydroborate; TFA, trifluoroacetic acid; TMT, tandem mass tag; VLPs, virus-like particles

REFERENCES

- (1) Sundquist, W. I.; Kräusslich, H. G. HIV-1 assembly, budding, and maturation. *Cold Spring Harbor Perspect. Med.* **2012**, *2*, a015420.
- (2) Charlton Hume, H. K.; et al. Synthetic biology for bioengineering virus-like particle vaccines. *Biotechnol. Bioeng.* **2019**, *116*, 919–935.
- (3) Willms, E.; et al. Cells release subpopulations of exosomes with distinct molecular and biological properties. *Sci. Rep.* **2016**, *6*, 22519.
- (4) Reiter, K.; et al. Separation of virus-like particles and extracellular vesicles by flow-through and heparin affinity chromatography. *J. Chromatogr. A* **2019**, *1588*, 77.
- (5) Lee, Y.; EL Andaloussi, S.; Wood, M. J. A. Exosomes and microvesicles: extracellular vesicles for genetic information transfer and gene therapy. *Hum. Mol. Genet.* **2012**, *21*, R125–R134.

- (6) Valadi, H.; et al. Exosome-mediated transfer of mRNAs and microRNAs is a novel mechanism of genetic exchange between cells. *Nat. Cell Biol.* **2007**, *9*, 654–659.

- (7) Vlassov, A. V.; Magdaleno, S.; Setterquist, R.; Conrad, R. Exosomes: Current knowledge of their composition, biological functions, and diagnostic and therapeutic potentials. *Biochim. Biophys. Acta, Gen. Subj.* **2012**, *1820*, 940–948.

- (8) Scourfield, E. J.; Martin-Serrano, J. Growing functions of the ESCRT machinery in cell biology and viral replication. *Biochem. Soc. Trans.* **2017**, *45*, 613–634.

- (9) Chettimada, S.; et al. Exosome markers associated with immune activation and oxidative stress in HIV patients on antiretroviral therapy. *Sci. Rep.* **2018**, *8*, 7227.

- (10) Takahashi, A.; et al. Exosomes maintain cellular homeostasis by excreting harmful DNA from cells. *Nat. Commun.* **2017**, *8*, 15287.

- (11) Zhu, Y.; et al. A Comprehensive Proteomics Analysis Reveals a Secretory Path- and Status-Dependent Signature of Exosomes Released from Tumor-Associated Macrophages. *J. Proteome Res.* **2015**, *14*, 4319–31.

- (12) Sun, D.; et al. Exosomes are endogenous nanoparticles that can deliver biological information between cells. *Adv. Drug Delivery Rev.* **2013**, *65*, 342–347.

- (13) Ung, T. H.; Madsen, H. J.; Hellwinkel, J. E.; Lencioni, A. M.; Graner, M. W. Exosome proteomics reveals transcriptional regulator proteins with potential to mediate downstream pathways. *Cancer Sci.* **2014**, *105*, 1384–1392.

- (14) Simpson, R. J.; Jensen, S. S.; Lim, J. W. E. Proteomic profiling of exosomes: Current perspectives. *Proteomics* **2008**, *8*, 4083–4099.

- (15) Hessvik, N. P.; Llorente, A. Current knowledge on exosome biogenesis and release. *Cell. Mol. Life Sci.* **2018**, *75*, 193–208.

- (16) Pant, S.; Hilton, H.; Burczynski, M. E. The multifaceted exosome: Biogenesis, role in normal and aberrant cellular function, and frontiers for pharmacological and biomarker opportunities. *Biochem. Pharmacol.* **2012**, *83*, 1484–1494.

- (17) Simons, M.; Raposo, G. Exosomes – vesicular carriers for intercellular communication. *Curr. Opin. Cell Biol.* **2009**, *21*, 575–581.

- (18) Ellwanger, J. H.; Veit, T. D.; Chies, J. A. B. Exosomes in HIV infection: A review and critical look. *Infect., Genet. Evol.* **2017**, *53*, 146–154.

- (19) Florin, L.; Lang, T. Tetraspanin Assemblies in Virus Infection. *Front. Immunol.* **2018**, *9*, 1140.

- (20) Sims, B.; et al. Tetraspanin blockage reduces exosome-mediated HIV-1 entry. *Arch. Virol.* **2018**, *163*, 1683–1689.

- (21) Gutiérrez-Granados, S.; Cervera, L.; Gòdia, F.; Carrillo, J.; Segura, M. M. Development and validation of a quantitation assay for fluorescently tagged HIV-1 virus-like particles. *J. Virol. Methods* **2013**, *193*, 85–95.

- (22) Cheeks, M. C.; Edwards, A. D.; Arnot, C. J.; Slater, N. K. H. Gene transfection of HEK cells on supermacroporous polyacrylamide monoliths: A comparison of transient and stable recombinant protein expression in perfusion culture. *New Biotechnol.* **2009**, *26*, 289–299.

- (23) Wiśniewski, J. R.; Zougman, A.; Nagaraj, N.; Mann, M. Universal sample preparation method for proteome analysis. *Nat. Methods* **2009**, *6*, 359–362.

- (24) Martínez-Bartolomé, S.; et al. Properties of average score distributions of SEQUEST: the probability ratio method. *Mol. Cell. Proteomics* **2008**, *7*, 1135–45.

- (25) Bonzon-Kulichenko, E.; Garcia-Marques, F.; Trevisan-Herraz, M.; Vazquez, J. Revisiting peptide identification by high-accuracy mass spectrometry: problems associated with the use of narrow mass precursor windows. *J. Proteome Res.* **2015**, *14*, 700–710.

- (26) Navarro, P.; et al. General statistical framework for quantitative proteomics by stable isotope labeling. *J. Proteome Res.* **2014**, *13*, 1234–1247.

- (27) Trevisan-Herraz, M.; et al. SanXoT: a modular and versatile package for the quantitative analysis of high-throughput proteomics experiments. *Bioinformatics* **2019**, *35*, 1594–1596.

- (28) Garcia-Marques, F.; et al. A Novel Systems-Biology Algorithm for the Analysis of Coordinated Protein Responses Using Quantitative Proteomics. *Mol. Cell. Proteomics* **2016**, *15*, 1740–1760.
- (29) Navarro, P.; et al. General statistical framework for quantitative proteomics by stable isotope labeling. *J. Proteome Res.* **2014**, *13*, 1234–47.
- (30) García-Marqués, F.; et al. A Novel Systems-Biology Algorithm for the Analysis of Coordinated Protein Responses Using Quantitative Proteomics. *Mol. Cell. Proteomics* **2016**, *15*, 1740–60.
- (31) Ashburner, M.; et al. Gene Ontology: tool for the unification of biology. *Nat. Genet.* **2000**, *25*, 25–29.
- (32) The Gene Ontology Consortium.. Expansion of the Gene Ontology knowledgebase and resources. *Nucleic Acids Res.* **2017**, *45*, D331–D338.
- (33) Huang, D. W.; Sherman, B. T.; Lempicki, R. A Systematic and integrative analysis of large gene lists using DAVID bioinformatics resources. *Nat. Protoc.* **2009**, *4*, 44–57.
- (34) Huang, D. W.; Sherman, B. T.; Lempicki, R. A. Bioinformatics enrichment tools: paths toward the comprehensive functional analysis of large gene lists. *Nucleic Acids Res.* **2009**, *37*, 1–13.
- (35) Fabregat, A.; et al. The Reactome Pathway Knowledgebase. *Nucleic Acids Res.* **2018**, *46*, D649–D655.
- (36) Huang, D. W.; Sherman, B. T.; Lempicki, R. A. Systematic and integrative analysis of large gene lists using DAVID bioinformatics resources. *Nat. Protoc.* **2009**, *4*, 44–57.
- (37) Szklarczyk, D.; et al. The STRING database in 2017: quality-controlled protein-protein association networks, made broadly accessible. *Nucleic Acids Res.* **2017**, *45*, D362–D368.
- (38) Shannon, P.; et al. Cytoscape: A Software Environment for Integrated Models of Biomolecular Interaction Networks. *Genome Res.* **2003**, *13*, 2498–2504.
- (39) González-Domínguez, I.; Puente-Massaguer, E.; Cervera, L.; Gòdia, F. Quality assessment of virus-like particles at single particle level: A comparative study. *Viruses* **2020**, *12*, 223.
- (40) Schneider, C. A.; Rasband, W. S.; Eliceiri, K. W. NIH Image to ImageJ: 25 years of image analysis. *Nat. Methods* **2012**, *9*, 671–5.
- (41) Lavado-García, J.; Jorge, I.; Cervera, L.; Vázquez, J.; Gòdia, F. Multiplexed Quantitative Proteomic Analysis of HEK293 Provides Insights into Molecular Changes Associated with the Cell Density Effect, Transient Transfection, and Virus-Like Particle Production. *J. Proteome Res.* **2020**, *19*, 1085–1099.
- (42) Freund, A.; et al. Proteostatic Control of Telomerase Function through TRiC-Mediated Folding of TCAB1. *Cell* **2014**, *159*, 1389–1403.
- (43) Seo, S.; et al. BBS6, BBS10, and BBS12 form a complex with CCT/TRiC family chaperonins and mediate BBSome assembly. *Proc. Natl. Acad. Sci. U. S. A.* **2010**, *107*, 1488–1493.
- (44) Sheffield, V. C. The blind leading the obese: the molecular pathophysiology of a human obesity syndrome. *Trans. Am. Clin. Climatol. Assoc.* **2010**, *121*, 172–81.
- (45) Jin, H.; et al. The conserved Bardet-Biedl syndrome proteins assemble a coat that traffics membrane proteins to cilia. *Cell* **2010**, *141*, 1208–19.
- (46) Venereo-Sánchez, A.; et al. Characterization of influenza H1N1 Gag virus-like particles and extracellular vesicles co-produced in HEK-293SF. *Vaccine* **2019**, *37*, 7100–7107.
- (47) Steppert, P.; et al. Purification of HIV-1 gag virus-like particles and separation of other extracellular particles. *J. Chromatogr A* **2016**, *1455*, 93–101.
- (48) Decout, A.; et al. Rational design of adjuvants targeting the C-type lectin Mincle. *Proc. Natl. Acad. Sci. U. S. A.* **2017**, *114*, 2675–2680.
- (49) McKee, A. S.; Marrack, P. Old and new adjuvants. *Curr. Opin. Immunol.* **2017**, *47*, 44–51.
- (50) Akers, J. C.; Gonda, D.; Kim, R.; Carter, B. S.; Chen, C. C. Biogenesis of extracellular vesicles (EV): exosomes, microvesicles, retrovirus-like vesicles, and apoptotic bodies. *J. Neuro-Oncol.* **2013**, *113*, 1–11.
- (51) McConnell, R. E.; et al. The enterocyte microvillus is a vesicle-generating organelle. *J. Cell Biol.* **2009**, *185*, 1285–1298.
- (52) Muralidharan-Chari, V.; et al. ARF6-Regulated Shedding of Tumor Cell-Derived Plasma Membrane Microvesicles. *Curr. Biol.* **2009**, *19*, 1875–1885.
- (53) Chen, L.; Chen, R.; Kemper, S.; Brigstock, D. R. Pathways of production and delivery of hepatocyte exosomes. *J. Cell Commun. Signal.* **2018**, *12*, 343–357.
- (54) Gruenberg, J.; Stenmark, H. The biogenesis of multivesicular endosomes. *Nat. Rev. Mol. Cell Biol.* **2004**, *5*, 317–323.
- (55) Zöller, M. Tetraspanins: push and pull in suppressing and promoting metastasis. *Nat. Rev. Cancer* **2009**, *9*, 40–55.
- (56) Hemler, M. E. Tetraspanin Proteins Mediate Cellular Penetration, Invasion, and Fusion Events and Define a Novel Type of Membrane Microdomain. *Annu. Rev. Cell Dev. Biol.* **2003**, *19*, 397–422.
- (57) Hurley, J. H. ESCRT complexes and the biogenesis of multivesicular bodies. *Curr. Opin. Cell Biol.* **2008**, *20*, 4–11.
- (58) Fujii, K.; Hurley, J. H.; Freed, E. O. Beyond Tsg101: the role of Alix in ‘ESCRTing’ HIV-1. *Nat. Rev. Microbiol.* **2007**, *5*, 912–916.
- (59) McCullough, J.; Fisher, R. D.; Whitby, F. G.; Sundquist, W. L.; Hill, C. P. ALIX-CHMP4 interactions in the human ESCRT pathway. *Proc. Natl. Acad. Sci. U. S. A.* **2008**, *105*, 7687–7691.
- (60) Pincetic, A.; Leis, J. The Mechanism of Budding of Retroviruses From Cell Membranes. *Adv. Virol.* **2009**, *2009*, 6239691–6239699.
- (61) Gould, S. J.; Booth, A. M.; Hildreth, J. E. K. The Trojan exosome hypothesis. *Proc. Natl. Acad. Sci. U. S. A.* **2003**, *100*, 10592–10597.
- (62) Nguyen, D. G.; Booth, A.; Gould, S. J.; Hildreth, J. E. K. Evidence That HIV Budding in Primary Macrophages Occurs through the Exosome Release Pathway. *J. Biol. Chem.* **2003**, *278*, 52347–52354.
- (63) Kramer, B.; et al. HIV interaction with endosomes in macrophages and dendritic cells. *Blood Cells. Blood Cells, Mol., Dis.* **2005**, *35*, 136–142.
- (64) von Schwedler, U. K.; et al. The protein network of HIV budding. *Cell* **2003**, *114*, 701–713.
- (65) Meng, B.; Lever, A. M. Wrapping up the bad news: HIV assembly and release. *Retrovirology* **2013**, *10*, 5.
- (66) Cutter, A. R.; Hayes, J. J. A brief review of nucleosome structure. *FEBS Lett.* **2015**, *589*, 2914–2922.
- (67) Cimarelli, A.; Sandin, S.; Höglund, S.; Luban, J. Basic residues in human immunodeficiency virus type 1 nucleocapsid promote virion assembly via interaction with RNA. *J. Virol.* **2000**, *74*, 3046–57.
- (68) Muriaux, D.; Mirro, J.; Harvin, D.; Rein, A. RNA is a structural element in retrovirus particles. *Proc. Natl. Acad. Sci. U. S. A.* **2001**, *98*, 5246–5251.
- (69) Fuenmayor, J.; Cervera, L.; Gòdia, F.; Kamen, A. Extended gene expression for Gag VLP production achieved at bioreactor scale. *J. Chem. Technol. Biotechnol.* **2019**, *94*, 302–308.
- (70) Cervera, L.; Gonzalez-Dominguez, I.; Segura, M. M.; Godia, F. Intracellular characterization of Gag VLP production by transient transfection of HEK 293 cells. *Biotechnol. Bioeng.* **2017**, *114*, 2507–2517.
- (71) Gutiérrez-Granados, S.; Cervera, L.; Segura, M. L.; Wölfel, J.; Gòdia, F. Optimized production of HIV-1 virus-like particles by transient transfection in CAP-T cells. *Appl. Microbiol. Biotechnol.* **2016**, *100*, 3935–3947.
- (72) Lavado-García, J.; Cervera, L.; Gòdia, F. An alternative perfusion approach for the intensification of virus-like particle production in HEK293 cultures. *Front. Bioeng. Biotechnol.* **2020**, *8*, 617.
- (73) Fuenmayor, J.; Cervera, L.; Rigau, C.; Gòdia, F. Enhancement of HIV-1 VLP production using gene inhibition strategies. *Appl. Microbiol. Biotechnol.* **2018**, *102*, 4477–4487.
- (74) Seifalian, A.; De La Peña, H.; Seifalian, A. M. The application of exosomes as a nanoscale cancer vaccine. *Int. J. Nanomed.* **2010**, *5*, 889.

(75) Tohidi, F.; Sadat, S. M.; Bolhassani, A.; Yaghobi, R. Construction and Production of HIV-VLP Harboring MPER-V3 for Potential Vaccine Study. *Curr. HIV Res.* **2018**, *15*, 434–439.

(76) Chea, L. S.; Amara, R. R. Immunogenicity and efficacy of DNA/MVA HIV vaccines in rhesus macaque models. *Expert Rev. Vaccines* **2017**, *16*, 973–985.

(77) Pereira Aguilar, P.; et al. Polymer-grafted chromatography media for the purification of enveloped virus-like particles, exemplified with HIV-1 gag VLP. *Vaccine* **2019**, *37*, 7070–7080.

(78) Rulli, S. J.; et al. Selective and Nonselective Packaging of Cellular RNAs in Retrovirus Particles. *J. Virol.* **2007**, *81*, 6623–6631.

(79) Khorchid, A.; Halwani, R.; Wainberg, M. A.; Kleiman, L. Role of RNA in Facilitating Gag/Gag-Pol Interaction. *J. Virol.* **2002**, *76*, 4131–4137.